



PERGAMON

Journal of Structural Geology 25 (2003) 1597–1613

**JOURNAL OF
STRUCTURAL
GEOLOGY**

www.elsevier.com/locate/jsg

Intragranular dynamic recrystallization in naturally deformed calcite marble: diffusion accommodated grain boundary sliding as a result of subgrain rotation recrystallization

Michel Bestmann, David J. Prior*

Department of Earth Sciences, Liverpool University, Brownlow Street, Liverpool L69 3GP, UK

Received 25 March 2002; received in revised form 3 December 2002; accepted 5 December 2002

Abstract

Intragranular microshear zones within a greenschist facies calcite marble were studied to try to constrain better the processes of dynamic recrystallization as well as the deformation processes that occur within newly recrystallized grains. Intragranular recrystallized grains within large, twinned calcite porphyroclasts can be related to the host from which they have recrystallized and are the focus of an electron backscatter diffraction study. Lattice distortions, low angle boundaries and some high angle boundaries ($> 15^\circ$) in the micros shears within a porphyroclast have the same misorientation axes suggesting that deformation occurred by climb-accommodated dislocation creep involving subgrain rotation recrystallization. Changes in the ratio of host and twin domain, as the deformation zone is entered, show that twin boundary migration also occurred. Recrystallized grains have similar sizes (10–60 μm) to subgrains, suggesting that they formed by subgrain rotation. However, within the intragranular microshear zones the misorientations between recrystallized grains and porphyroclasts are considerably larger than 15° and misorientation axes are randomly oriented. Moreover recrystallized grain orientations average around the porphyroclast orientation. We suggest that the recrystallized grains, once formed, are able to deform partly by diffusion accommodated grain boundary sliding, which is consistent with predictions made from lab flow laws.

© 2003 Elsevier Science Ltd. All rights reserved.

Keywords: Calcite; Electron backscatter diffraction (EBSD); Misorientation; Orientation map; Subgrain rotation recrystallization; Grain boundary sliding

1. Introduction

The process of dynamic recrystallization plays a fundamental role in controlling the rheology and microstructures of rocks, especially in high strain zones (e.g. Urai et al., 1986). However, many details remain obscure. For example, the progressive change of crystallographic orientation during formation of new grains and the development of orientation relationships across (sub)grain boundaries during progressive plastic strain are not yet well documented (e.g. Leiss and Barber, 1999). Analysis of misorientation distributions is a powerful tool to quantify microstructural features and to constrain deformation processes and history (e.g. Fliervoet and White, 1995; Trimby et al., 1998, 2000; Kruse et al., 2001; Spiess et al., 2001; Wheeler et al., 2001; Prior et al., 2002). The data required for misorientation

analysis can now be obtained routinely and rapidly by electron backscatter diffraction (EBSD). Orientation maps constructed from EBSD data (Adams et al., 1994; Kunze et al., 1994) have enormous potential in microstructural studies (Prior et al., 2002) because different models for microstructural evolution predict particular relationships between adjacent grains. For example, microstructures resulting from subgrain rotation recrystallization should show a strong crystallographic relationship between adjacent grains (Lloyd et al., 1997; Wheeler et al., 2001). The misorientation between two lattices can be expressed by a rotation axis and rotation angle (Randle and Ralph, 1986; Mainprice et al., 1993; Wheeler et al., 2001). Although the orientation mapping does not provide the orientation of the boundary/interface plane to describe fully the geometry, the misorientation analysis alone helps to discriminate the role of various processes in forming microstructures (Fliervoet et al., 1999; Leiss and Barber, 1999; Prior et al., 1999; Kruse et al., 2001; Prior et al., 2002).

* Corresponding author. Tel.: +44-151-794-5193; fax: +44-151-794-5196.

E-mail address: davep@liv.ac.uk (D. Prior).

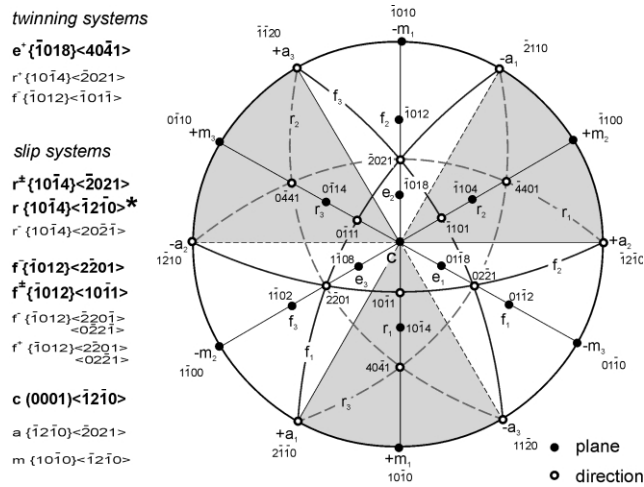


Fig. 1. Stereographic (upper hemisphere, equal angle) projection of calcite showing the important planes and directions, including the known slip systems (after De Bresser and Spiers, 1997). Bold letters highlight important slip systems. Asterisk indicates a slip system proposed by Pieri et al. (2001) but not experimentally verified. Shading illustrates trigonal symmetry point group $\bar{3}m$ of calcite.

This study focuses on the initial process of dynamic recrystallization in calcite. Carbonate rich rocks record ductile deformation in the upper crust and localized plastic flow in carbonate shear zones is an important aspect of lithosphere dynamics (e.g. Bestmann et al., 2000). Fig. 1 shows the crystallography and the known slip systems of calcite. The most favoured sites for the initiation of strain-induced recrystallized grains are old grain boundaries (e.g. Urai et al., 1986), but in such cases the crystallographic dependence of the new recrystallized grains with respect to the two different adjacent old grains may be ambiguous. In the current study, only intragranular (rather than intergranular) microshear zones were analysed. In these cases,

the new grains can be related to their host grain. The samples are from a monomineralic calcite marble shear zone located on Thassos Island, Greece. The microstructural and crystallographic evolution of the greenschist facies shear zone have been constrained by Bestmann et al. (2000). Two different microshear zones within coarse grained calcite porphyroclasts were analysed using orientation and misorientation analysis based on EBSD data.

2. Methods

2.1. Sample preparation

Polished blocks of two samples from the same shear zone profile were cut parallel to the shear direction and perpendicular to the shear zone boundary. Sample blocks were polished with diamond paste before a final stage of SYTON-polishing (Fynn and Powell, 1979; Prior et al., 1996). Reflected light microscopy was used to select microstructures for EBSD analysis (Fig. 2). To avoid charging effects, sample surfaces were coated with the thinnest possible layer of carbon.

2.2. Data acquisition

Full crystallographic orientation data were obtained from automatically indexed EBSD patterns collected in a CamScan X500 Crystal Probe fitted with a thermionic field emission gun and a FASTRACK stage. EBSD patterns were obtained using a 20 kV acceleration voltage and a beam current between 8 and 12 nA (dependent on the carbon coating) at a working distance of 25 mm. Samples were mapped by stage movement on a grid with a fixed step size of 2 μm . This step size ensured that each (sub)grain

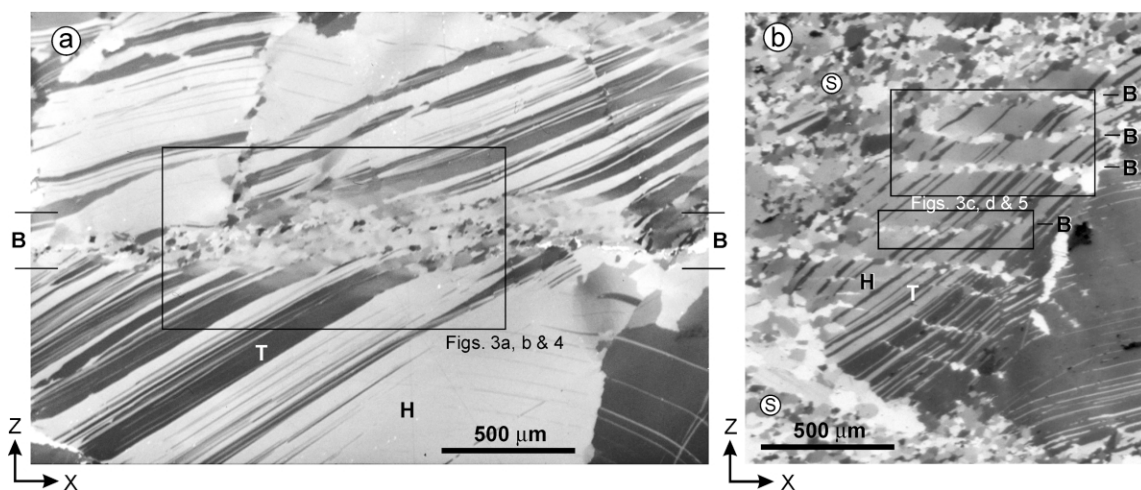


Fig. 2. Reflected light micrographs to show the microstructures of two analysed intragranular microshear zones. (a) Microstructure A shows a 200 μm thick horizontal band (B) of patchy undulatory extinction crosscutting calcite porphyroclast. The porphyroclast shows one dominant twin set (T: dark colours) within the host orientation (H: light colour). (b) Microstructure B contains sharp, well-developed parallel oriented bands (B) of small grains cutting through the host grain. The porphyroclast is surrounded by a matrix of small grains (S). Boxes show locations analysed by EBSD scans.

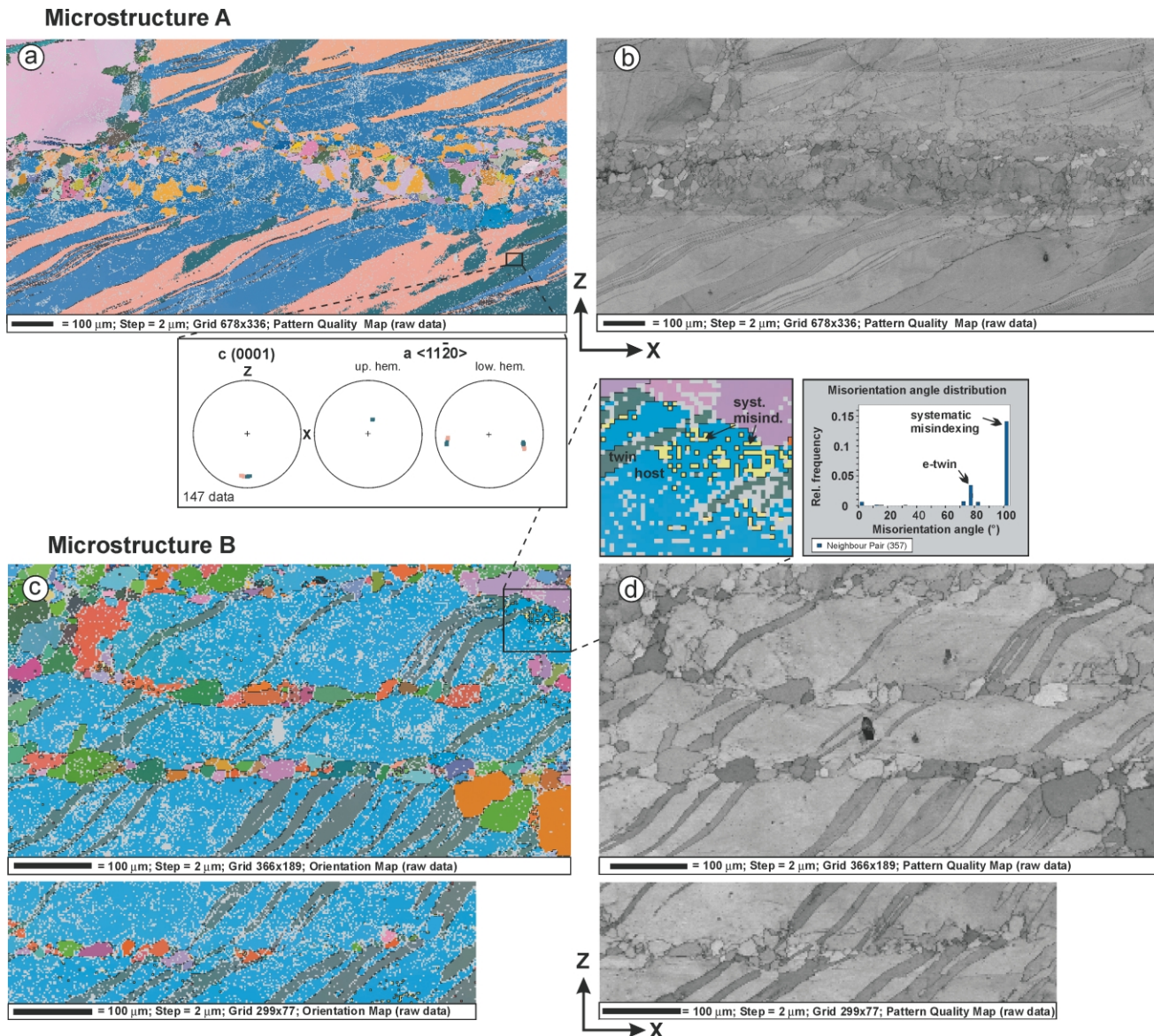


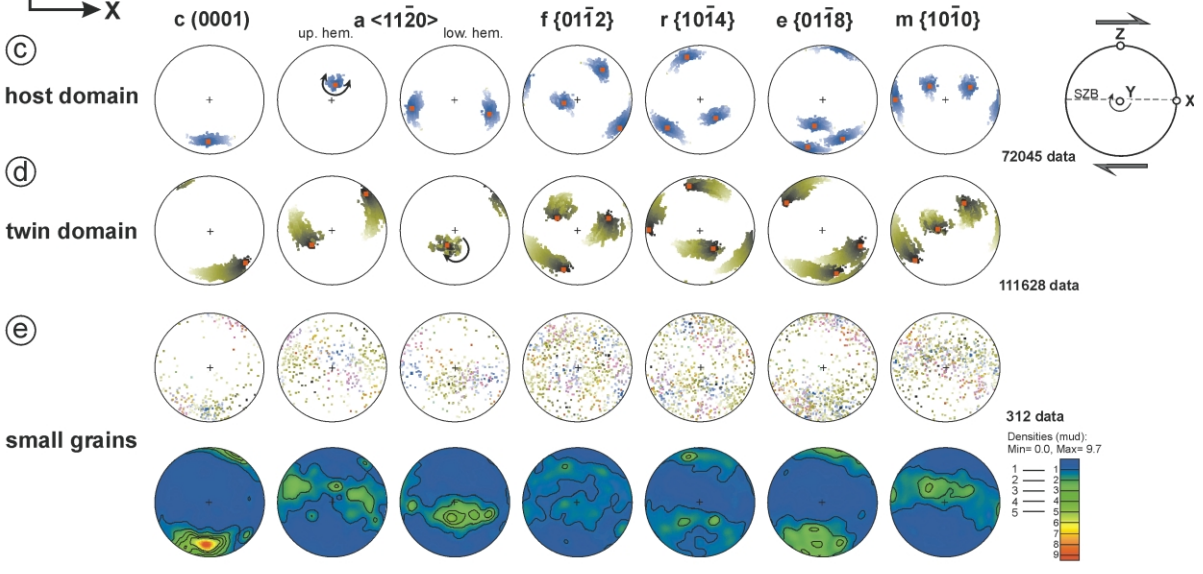
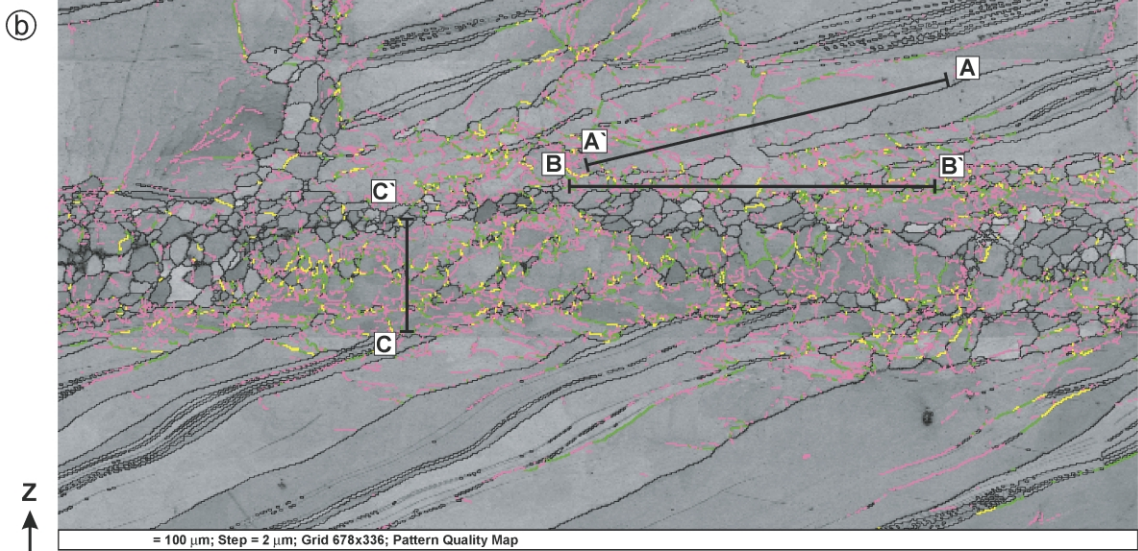
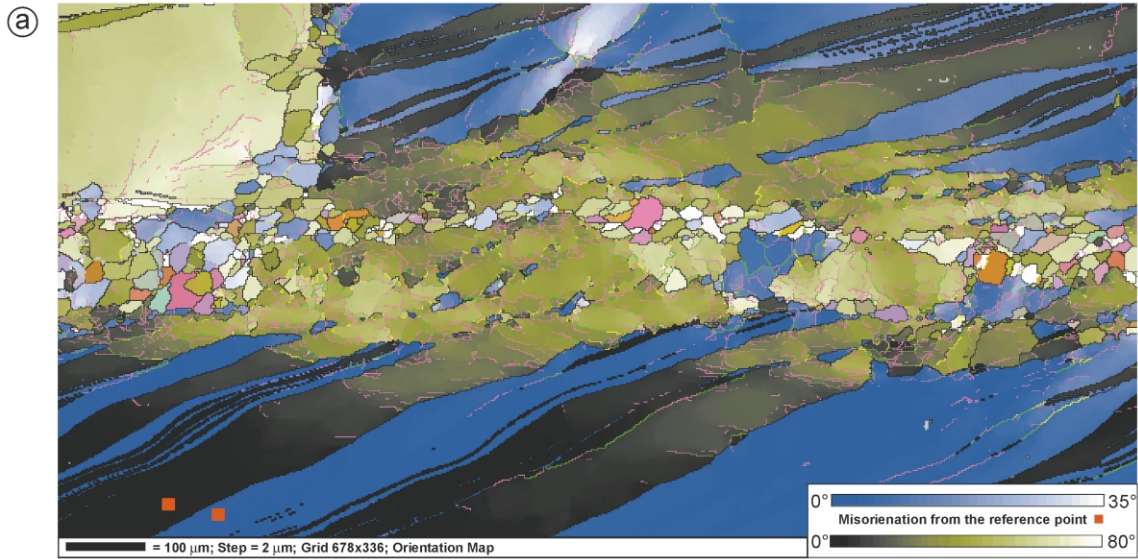
Fig. 3. Raw orientation and pattern quality maps of the analysed microstructures. (a) and (c) In the orientation maps each pixel is colour-coded with respect to its Euler angles (see text). Data are on a grid with 2 μm spacing. Light grey areas are points that were not indexed. Black lines are drawn between any two adjacent points with a misorientation $> 15^{\circ}$. The blow up in (c) shows the problem with systematic misindexing related to a particular EBSD pattern (see text). (b) and (d) Pattern quality (band contrast) maps. Dark pixels have poor pattern quality, bright pixels show good pattern quality. Changes in grey level across horizontal lines is related to user controlled brightness correction of the EBSD signal during the automatic run.

($d \sim 10\text{--}60 \mu\text{m}$) contained several measurement points. The stored EBSD patterns were indexed using the program CHANNEL 4.2 from HKL technology. The centre of 6–8 Kikuchi bands were detected automatically using the Hough transform routine (Adams et al., 1993). The solid angles calculated from the patterns were compared with a calcite match unit containing 80 reflectors to index the pattern. Average measuring time per individual orientation analysis was 0.5 s and average non-indexing (EBSD patterns that could not be indexed) ranges between 15 and 22%. Using a smaller number of bands in the diffraction pattern could reduce the percentage of non-indexing but increases dramatically the amount of systematic misindexing.

2.3. Data display

EBSD data are usefully presented as maps. In the orientation maps (Figs. 3a and c, 4a and 5a), the colour of every pixel is generated by superposition of three colour channels (red, green and blue), which are assigned the values of the three Euler angles ϕ_1 , Φ , ϕ_2 of each measuring point. Because of the way that Euler angles are defined (Bunge, 1965) sudden changes of colour can occur that do not correspond to large changes in orientation (see blow up of Fig. 3a). In pattern quality maps (Figs. 3b and d, 4b and 5b), grey shades relate to a quantitative image analysis parameter of the EBSD pattern. Since these pattern

Microstructure A



quality maps reproduce surface damage and misorientation boundaries, they are a useful tool to verify the reliability of the orientation maps. The misorientation angle between adjacent points was calculated by selecting the minimum misorientation angle and its corresponding axis from all possible symmetric variants (Randle and Ralph, 1986; Mainprice et al., 1993; Wheeler et al., 2001). Boundaries related to different misorientation intervals are presented as coloured lines on the orientation maps. An angle of 2° was chosen as a minimum misorientation that can be reliably identified using the EBSD method (Prior, 1999; Humphreys et al., 2001).

2.4. Data processing

Raw orientation maps (Fig. 3a and c) are processed to provide a more complete reconstruction of the microstructure and to remove erroneous data (Figs. 4 and 5). Non-indexed points are concentrated at grain boundaries because that is where pattern quality is low (Fig. 3b and d). This will cause an underestimation of real boundaries when misorientation analysis of neighbouring analysis points is applied (Prior et al., 2002). CHANNEL 4.2 software provides a simple algorithm to replace these non-indexed measuring points by the most common neighbouring orientation. The degree of processing required to fill non-indexed data points without introducing artefacts was tested carefully.

Because the step size is much smaller than the grain size, non-systematic errors can be identified as individual data points that are different from all surrounding data points. An automatic filter removes such points. Data points that are incorrectly indexed in a systematic manner are more problematic. These occur where the stronger diffraction bands in two different patterns are sufficiently similar to be indistinguishable by the indexing software. A systematically misindexed point is an incorrect solution that is rotated about a specific angle/axis pair from the correct solution (e.g. $103\text{--}104^\circ$ around a $\langle -4401 \rangle$ or $\langle -202 - 1 \rangle$ axis relative to neighbouring points; blow up of Fig. 3c). The most common orientation (light blue pixels in Fig. 3c) will be used as the reference orientation towards which misindexed pixels (yellow pixels in Fig. 3c) will be rotated. This correction procedure will not introduce artefacts as long as there are no significant real boundaries that have the same angle/axis pair as the systematic misindexing (Prior

et al., 2002). The correction procedure assumes that systematically misindexed points will be less significant than correctly indexed points.

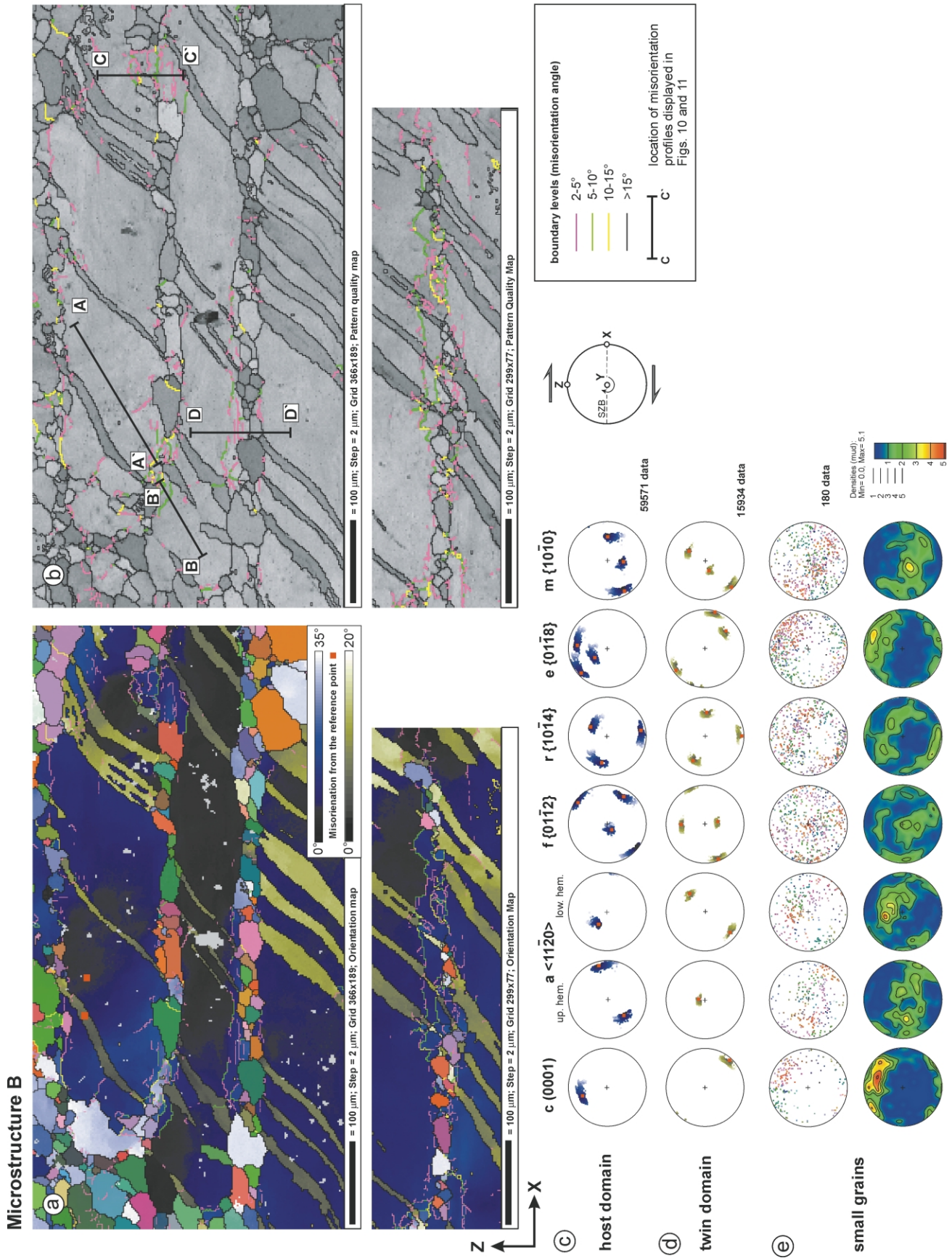
3. Results

3.1. Calcite microstructures

The samples examined in this paper are from a 3-m-wide marble shear zone on the Isle of Thassos, Greece (Bestmann et al., 2000). Both samples (C24 and C12.1; see Bestmann (2000) for details) are monomineralic and coarse-grained (1–3 mm) with a high density of twin lamellae and one dominant twin set. Many of the twins are lensoid, bent or tapered in the interior of the grains. Varying amounts of small grains along grain boundaries, and sometimes within porphyroclasts, indicate that these samples are protomylonites. The protolith marble outside of the shear zone contains no small grains. Therefore, these small grains can be interpreted as new grains related to the deformation during the shear zone evolution (see also Bestmann et al., 2000). Coarse grains ($d \sim 1\text{--}3$ mm) with internal bands of small grains ($d \sim 10\text{--}60$ μm) were chosen for analysis. This microstructure guarantees that the small grains are related to their host coarse grain and do not relate to grains from the third dimension above or below the observed section, as could be the case for small grains developed along grain boundaries between two different grains. We define these new small grains as areas surrounded completely by high angle boundaries. The value of misorientation chosen to define a high angle boundary is arbitrary (Urai et al., 1986). We have chosen to define boundaries with a misorientation angle larger than 15° as high angle boundaries.

Within the coarse host grains, the small grains are arranged in bands. The traces of these crosscutting bands are oriented subparallel to the shear zone boundary that is used as the kinematic reference plane (Bestmann et al., 2000). The grains within these bands have sharp and straight grain boundaries and a preferred grain shape orientation (SPO). Long axes are between 10 and 60 μm in length and the grains have an average aspect ratio of 1:1.8. The long axes are preferentially oriented at around 20° anticlockwise to the trace of the crosscutting band.

Fig. 4. Processed map of microstructure A. The map is processed to remove erroneous data (see text). (a) Orientation maps. Grey pixels are non-indexed points, which have not been removed during processing. The pixels of the host (blue) and twin (olive green) orientation domains are colour shaded according to their angular misorientation from the points marked as red squares, one in twin and one in host. Small grains, which are oriented within these defined orientation ranges are colour coded in the same way. All other pixels are colour coded with respect to their Euler angles (see text). Boundary misorientations are colour coded (see key in Fig. 5). (b) To highlight boundary misorientations, they are plotted on the pattern quality map as thicker lines than in (a) and with the same colour code. (c)–(e) Pole figures (equal area upper hemisphere stereoplots) of the host domain, twin domain and the small grains within the intracrystalline bands crosscutting the porphyroclasts, as marked in Fig. 1. Points in the pole figures have colours that correspond to the orientation maps. In pole figures of (c) and (d) reference orientations for colour shading for the twin and host domain are displayed as red squares. Dispersion axes and sense of rotation are given. Sample reference system and sense of shear of the bulk shear zone are shown (SZB, shear zone boundary; Y, kinematic rotation axis of bulk shear zone geometry).



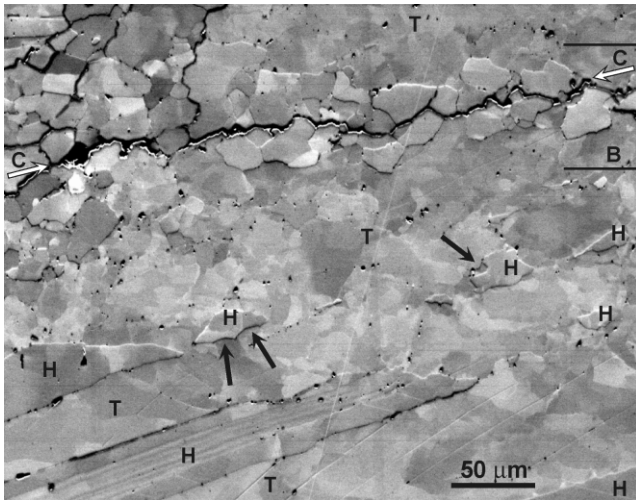


Fig. 6. SEM orientation contrast image of the highly-distorted area from microstructure A. Black arrows mark some relicts of the host domain (H) showing concave shaped grain boundaries with respect to the surrounding twin orientation (T). In the upper part of the image the band (B) of small grains is visible. A late crack (C + white arrows) along grain boundaries of small grains cuts through that band.

Two contrasting microstructures (Fig. 2) were selected for EBSD analysis. The porphyroclast in microstructure A (sample C24 of Bestmann et al. (2000)) is surrounded by other coarse grains, whereas the porphyroclast in microstructure B (sample C12.1, Bestmann et al. (2000)) is embedded in a matrix of small grains, with an average grain size of 10–30 μm . The main difference between the two microstructures is visible under the reflected light microscope. Microstructure A shows diffuse orientation contrast in an area around the band of small grains (Fig. 2a). In contrast, microstructure B is characterised by parallel, very sharp bands of small grains cutting through the host grain (Fig. 2b).

3.2. Orientation maps

The raw orientation maps (Fig. 3a and c) reproduce reflected light (Fig. 2) and pattern quality maps (Fig. 3b and d) microstructures accurately, apart from a small amount of systematic misindexing (Fig. 3c). In the processed orientation maps (Figs. 4a and 5a) the host grain and the twin set within the host are colour coded to highlight gradual orientation changes within the porphyroclasts (see figure caption). The orientation domain that dominates the grain is defined as the host domain.

3.2.1. Microstructure A

The orientation map of microstructure A shows that the lattice of the porphyroclast is heterogeneously deformed

(Fig. 4a). The outer part of the microstructure shows a gradual lattice bending towards a highly-distorted area surrounding the crosscutting band of small grains. A high density of low angle boundaries is observed in the highly-distorted area of the porphyroclast. Also some individual high angle boundaries (up to 40°) are developed within the host and twin orientation domain. The subgrain domains, surrounded by low angle boundaries have sizes between 10 and 70 μm and show gradual changes in orientation internally. In contrast the small ($d \sim 10\text{--}60 \mu\text{m}$) grains surrounded by high angle boundaries, which occur in the centre of the distorted area, show homogeneous intracrystalline orientation (orientation changes by less than the measurement accuracy of 1°). Only some of the small grains contain low angle boundaries.

The host (Fig. 4c) and especially the twin (Fig. 4d) domain show a strong dispersion around one of the a -axes, located near the centre of the pole figure. Around this axis the twin orientation (Fig. 4d) undergoes a clockwise rotation of up to 80° from the less distorted area towards the highly-distorted area, whereas the host orientation (Fig. 4c) deviates only about 30° (for angles compare color reference table; see inset in Fig. 4a). The twin domain (olive green), dominates the highly-distorted area even though both of the orientation domains show similar volume in parts of the porphyroclast outside of the microshear zone. Only isolated remnants of the host domain with concave grain boundaries occur within this highly-distorted area (Fig. 6).

The CPO of the small grains (Fig. 4e) scatters statistically around the orientation of the surrounding distorted area. In detail the small grains can be described as the superposition of a distribution centred on the twin orientation and a weaker distribution centred on the host orientation. The statistical average orientation of the small grains is the same as the orientation of the twin domain in the distorted zone, which is rotated 80° clockwise from the orientation of the relative undeformed twin domain outside the microshear zone.

3.2.2. Microstructure B

Microstructure B contains several distinct orientation domains (Fig. 5a). The host grain and its twin set show some internal distortion, especially close to the crosscutting bands. The interiors of the small grains ($d \sim 10\text{--}50 \mu\text{m}$) are crystallographically relatively homogeneous. Low angle boundaries are rare within the small grains. Within the host/twin domains there are a few low angle boundaries. These lie close to the crosscutting bands, especially in the host orientation domain. A higher density of low angle boundaries is located in distinct areas of the band where fewer small grains occur. The traces of these low angle

boundaries are on average (sub)parallel to the crosscutting bands. The few definable domains surrounded by low angle boundaries have sizes of 10–70 μm .

The distortion of host and twin is also illustrated in the pole figures (Fig. 5c and d). The rotation axis of the dispersion pattern is located near the centre of the pole figure, somewhere close to one of the *a*-axes of both host and twin and the pole to one of the *f*-planes and/or *m*-planes of both host and twin. The range of misorientation dispersion with respect to the reference orientation is $\sim 35^\circ$ for the host domain and $\sim 15^\circ$ for the twin domain.

The small grains in the crosscutting bands show a variety of orientations. The CPO can be described as the superposition of a distribution centred on the host orientation and a weaker distribution centred on the twin orientation. With respect to the undeformed parts of the grain the CPO is rotated by $\sim 25^\circ$ in a clockwise sense about an axis located in the centre of the pole figures (Fig. 5e).

3.3. Misorientation analysis

3.3.1. Misorientation angle distribution

Random-pair misorientation distributions differ from the

theoretical curve for a random orientation distribution (Fig. 7), due to the strong CPO. For both microstructures, the neighbour-pair misorientation angle distributions are bimodal and different from the random-pair misorientation distributions (Fig. 7). The peak at about $75\text{--}80^\circ$ is related to the twinning system in calcite.

The distribution of misorientations measured between small grains and neighbouring host grains is nearly bell-shaped for both microstructures. These boundaries are characterised by relatively high misorientation angles, peaking at $45\text{--}65^\circ$ for microstructure A and at $35\text{--}80^\circ$ for microstructure B. The lack of misorientations less than 15° is an artefact due to our definition of individual orientation domains. For microstructure A the distribution of misorientations within the population of small grains is quite similar to the distribution of misorientations between small grains and host grains and the random-pair misorientation angle distribution is the same as the neighbour-pair misorientation angle distribution (Fig. 7a). Therefore there is no evidence for the existence of any preferred misorientation between small grains and host grain, and between nearest neighbour-pairs within the population of small grains (see also Wheeler et al., 2001).

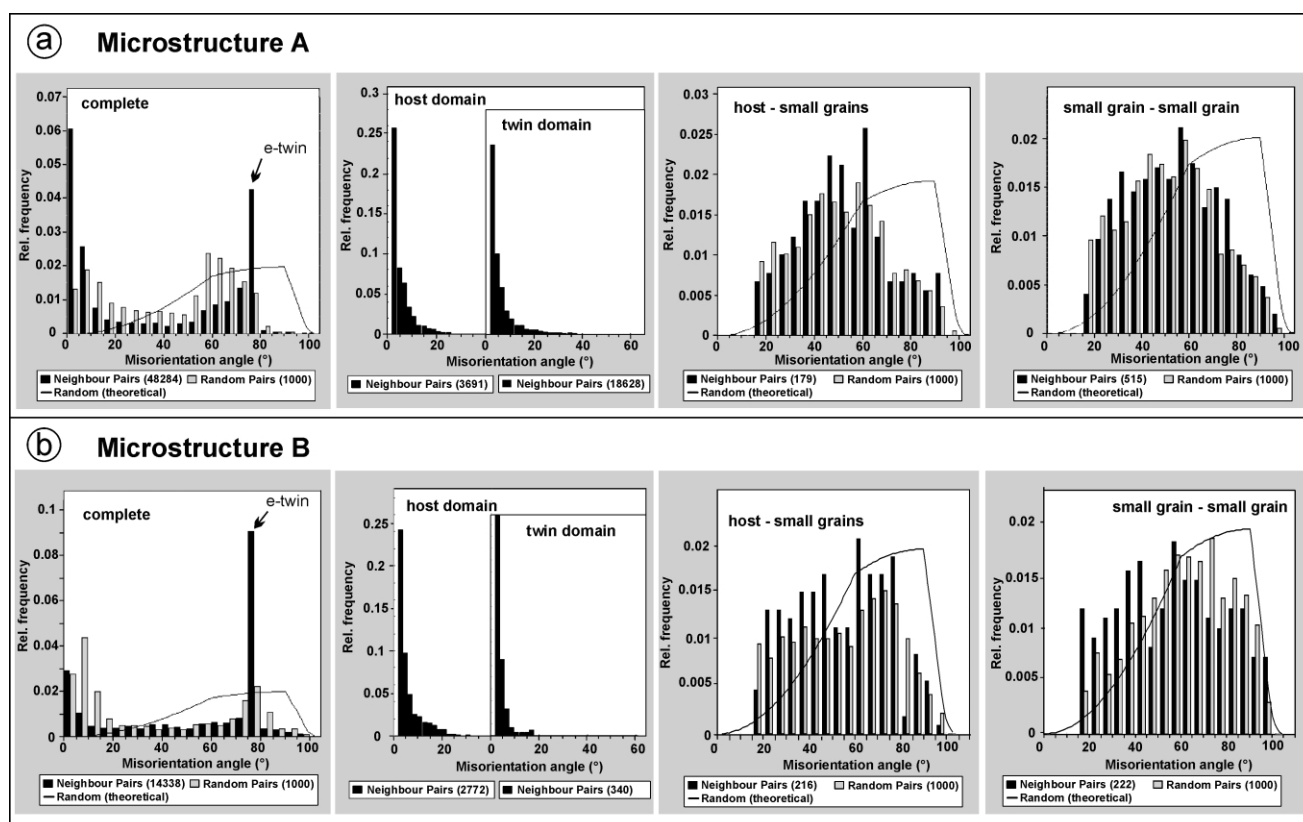
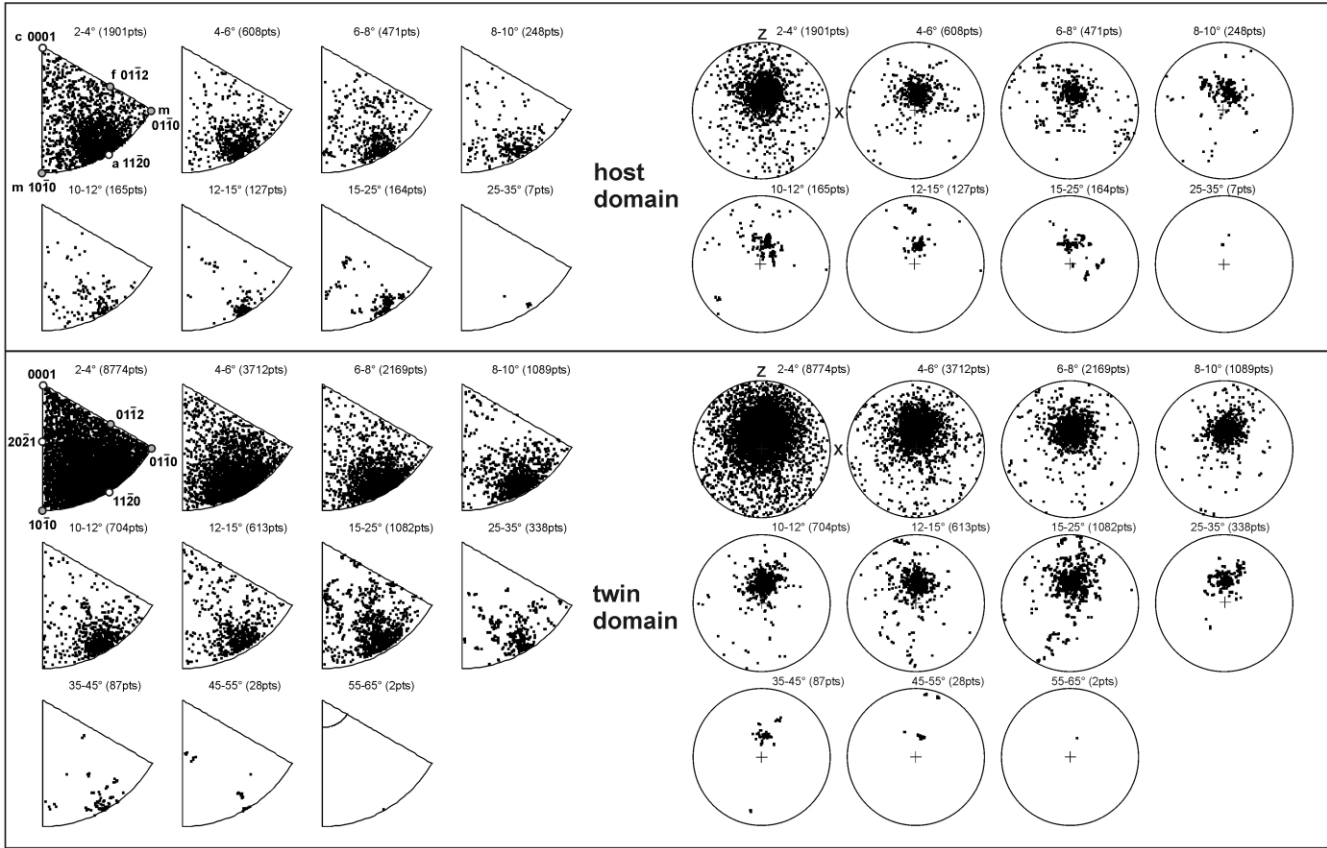


Fig. 7. Distribution of misorientation angles for (a) microstructure A and (b) microstructure B. Data are presented as histogram plots for the complete porphyroclast (twin + host + small grains), host domain, twin domain, host vs. small grains, and within the population of small grains. The last two plots are calculated from manually selected data, the others are calculated automatically (by using the grain reconstruction routine in the CHANNEL 4.2 software) from all neighbouring pixels with a misorientation angle $> 2^\circ$. Dark columns are the misorientations across boundaries between neighbouring data points (automatically collected) or neighbouring domains (manually selected). Pale columns are the misorientations between randomly picked pairs of grains (see Wheeler et al., 2001). The theoretical curve for a random orientation distribution is given (see Wheeler et al., 2001).

(a) Microstructure A



(b) Microstructure B

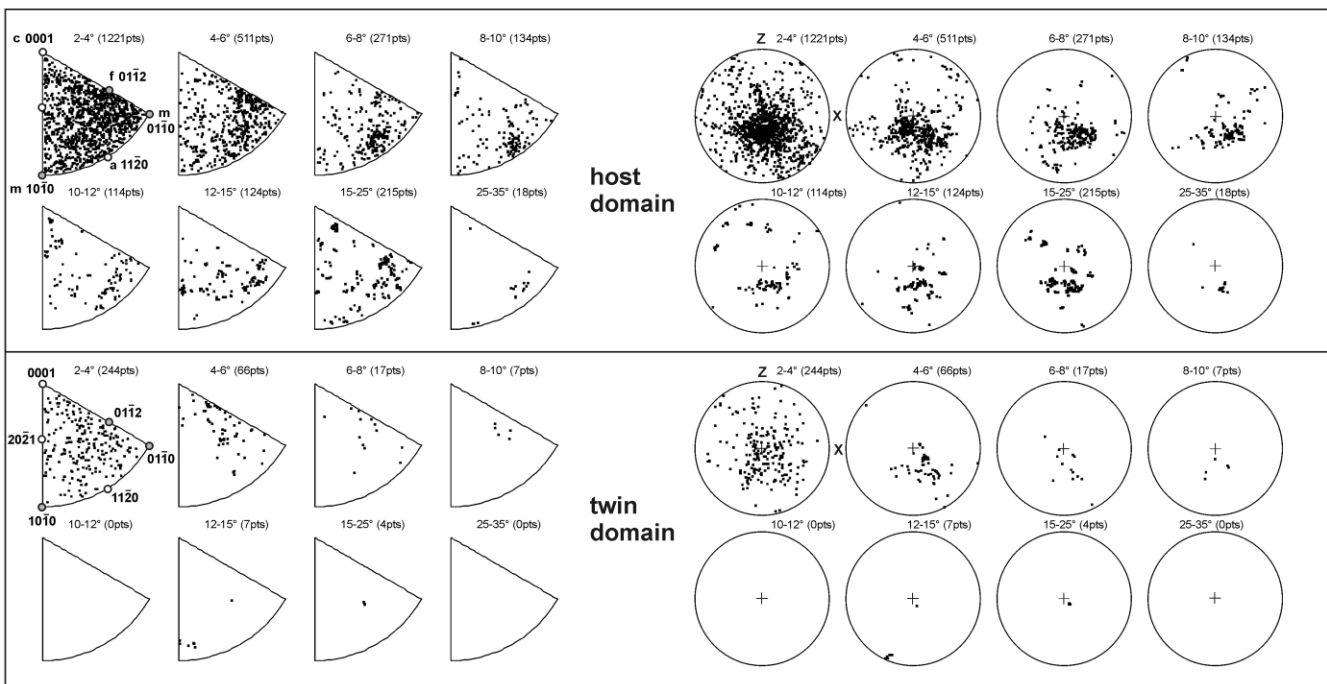


Fig. 8. Distribution of misorientation axes for (a) microstructure A and (b) microstructure B. Data for the host and twin domains are separated into different misorientation angle intervals. Left columns show misorientation axis related to the crystal reference frame as inverse pole figures IPF (equal area, upper hemisphere projection) and right columns with respect to the sample reference frame as pole figures (equal area, upper hemisphere projection). Important crystallographic directions (white circles) and planes (grey circles) are marked in the first IPF diagram. For each plot the number of data points (pts) is given.

Microstructure A

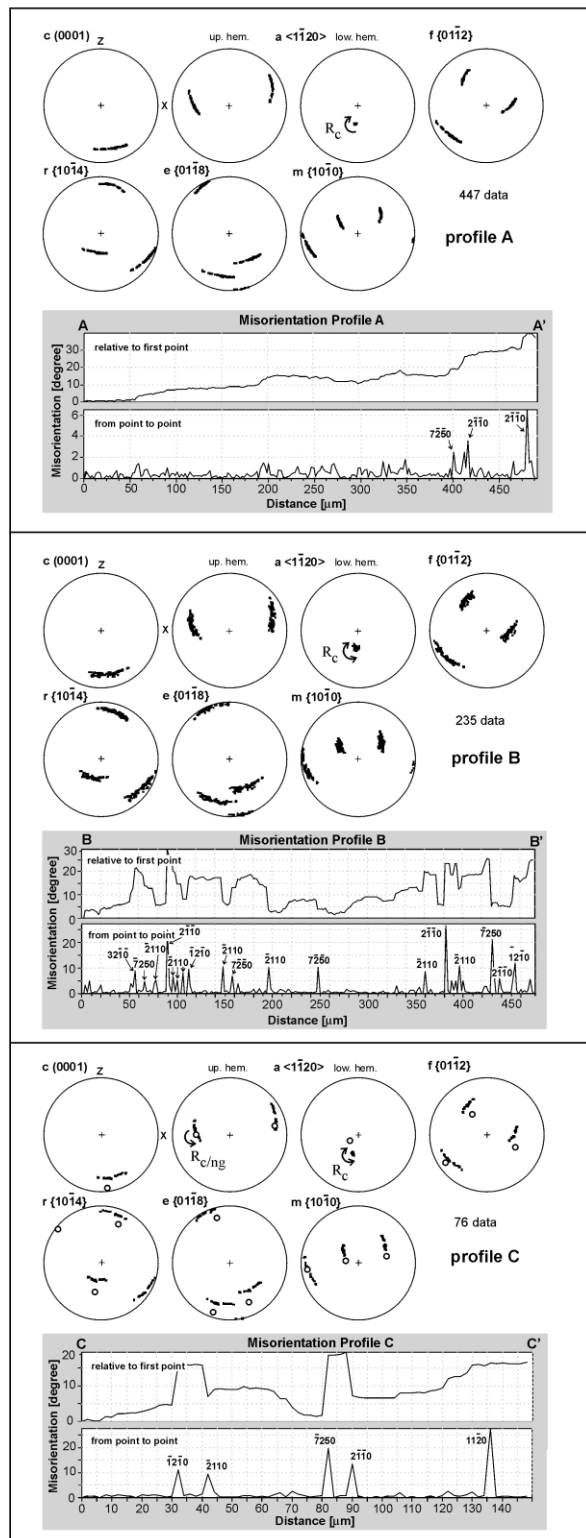


Fig. 9. Misorientation profiles within microstructure A. Change of orientation along lines of measurement are presented as dispersion patterns in pole figures (equal area, upper hemisphere). Misorientation axes and their sense of rotation are estimated from the dispersion pattern, if it was possible (R_c misorientation axis within porphyroclast; $R_{c/ng}$, $R_{c/sg}$ misorientation axis between porphyroclast/new grain or porphyroclast/sub-

3.3.2. Misorientation axis distribution

The analysis of misorientation axes was focussed on lattice distortion patterns within the deformed porphyroclast grains and the relationship between small grains and their host grains. Although an individual calculated misorientation axis for misorientation angles less than 20° can contain a significant error ($> 12^\circ$) a statistically representative data set is able to give reliable average misorientation axes for angles less than 10° (Prior, 1999). Misorientation axes with angles less than 5° should be treated with particular caution. However, the IPF and pole figure plots (Fig. 8) of the misorientation axes illustrate that a statistically representative data set can yield consistent misorientation axis data even for misorientations below 10° .

3.3.2.1. *Microstructure A.* Fig. 8a shows that the deformation of the host and the twin orientation domains of microstructure A is mainly controlled by a lattice rotations around a misorientation axis (sub)parallel to one of the crystallographic a -axes of calcite. Geographically the misorientation axes plot slightly above the centre of the pole figure, which represents the kinematic rotation axis of the shear zone (see Fig. 4).

Misorientation profiles show that the lattice is reoriented from the outer parts of the microstructure towards the centre of distortion by a gradual clockwise rotation around $\langle a \rangle$ (Fig. 9, profile A). However within the highly-distorted zone the distinct orientation sub-domains crossed by the misorientation profiles oscillate in a clockwise and/or anticlockwise sense around the a -axis ('relative to first point' diagram of profile B). Even when high angle boundaries (up to $\sim 30^\circ$) are crossed, the dispersion path and therefore the misorientation axis is consistent. In contrast, the crystallographic dispersion across boundaries between small grains and porphyroclast is not any more consistent (Fig. 9, profile C).

Statistically, the distribution of misorientation axes between host and small grains, as well as between neighbour-pairs of small grains themselves is almost uniform (Fig. 10a).

3.3.2.2. *Microstructure B.* The IPFs in Fig. 8a reveal that the distribution of misorientation axis is more heterogeneous compared with microstructure A. Lines of orientation measurements within the deformed porphyroclast show small circle dispersions around different misorientation axes (Fig. 11, profile B: rotation around $\langle a \rangle$, profile D: rotation around f -pole, profile A + C: rotation around m -pole). The degree of dispersion is dependent on the location of the misorientation profile, its orientation (horizontal, vertical or

grain). Open circles mark the orientation of new grains or specific subgrains. In corresponding graphs the continuous change of misorientation angle is displayed with respect to the first point and also from point to point. For pronounced misorientation boundaries the crystallographic indices of the misorientation axis are given. Location of profiles are given in Fig. 4.

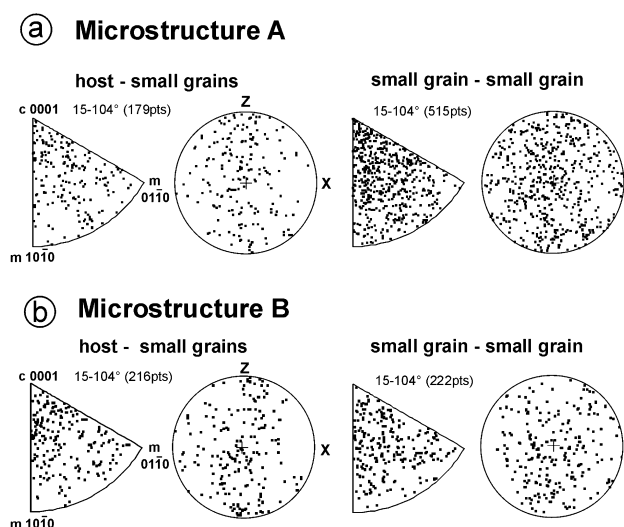


Fig. 10. (a) and (b) Distribution of misorientation axes constrained from manually selected (one per grain) data between host and new grains, as well between neighbour-pairs of new grains themselves. Misorientation angle interval is 15–104°. Misorientation axes are displayed as IPFs and pole figures (see Fig. 8).

diagonal) and length (Figs. 5b and 11). Subgrain boundaries crossed by individual misorientation profiles can influence the consistency of the dispersion path (profile A).

All of the three crystallographic directions ($\langle a \rangle$, $\{f\}$ and $\{m\}$) identified as misorientation axes have three crystallographic equivalent orientations related to the trigonal crystal symmetry of calcite (Fig. 1). Whichever one is oriented nearest to the pole figure centre (also the kinematic rotation axis of the sample reference system) is the one that acts as the misorientation axis (Fig. 11). These three specific $[a]$, $\{f\}$ and $\{m\}$ directions all plot in approximately in the same area, just below the centre of the pole figures (Fig. 11).

As in microstructure A, the misorientation axes for boundaries between small grains and host grains have almost a random distribution (Fig. 9b). This statistical observation is verified by individual misorientation profiles (Fig. 11). In general there is no continuous rotation from the host grain across high angle misorientation boundaries of individual small grains within the crosscutting band (profile D). The misorientation axes between neighbouring small grains are almost randomly distributed (Fig. 9b).

4. Discussion and interpretation

The tight crystallographic control upon misorientation axes associated with lattice distortion and boundaries within the porphyroclasts is best explained by a dislocation creep deformation mechanism coupled with recovery. The mechanisms for formation of the small grains are less obvious. This discussion is broken down into three major elements. Firstly the geometry of deformation within the

porphyroclasts is used to place constraints on the slip systems involved in the deformation. Secondly we discuss the recovery and recrystallization mechanisms that may have given rise to the development of new grains. Finally we address the rheological implication with respect to the concluded deformation mechanisms.

4.1. Identification of slip systems by misorientation analysis

Misorientation axes can be used to constrain important slip systems (Lloyd and Freeman, 1991; Prior et al., 1999, 2002; Leiss and Barber, 1999). A simple way to constrain dislocation slip systems responsible for crystal plastic deformation is to consider two end-member models (Trepied et al., 1980; Hull and Bacon, 1984): screw dislocations and edge dislocations. Screw dislocations build twist boundaries with misorientation axes perpendicular to the boundary plane, which is also the slip plane of the dislocation system. Edge dislocations build tilt boundaries. For minerals with orthorhombic and higher symmetry misorientation axes lie within the slip plane and normal to the slip direction whereas for lower symmetric minerals, e.g. for triclinic plagioclase the angle between the misorientation axis and the Burgers vector can differ from 90° (Kruse et al., 2001). In calcite, de Bresser (1991) showed that for the main slip systems (r - and f -slip), the rotation axis is expected to be perpendicular to the slip direction when only one slip system is active. For basal $\langle a \rangle$ slip this is not verified but is likely to be the same.

4.1.1. Microstructure A

In the deformed porphyroclast (Fig. 13), gradual lattice bending, low angle boundaries and a few high angle boundaries all share a misorientation axis parallel to a specific crystallographic a -axis and thus are likely produced by the same dislocation system (see also Prior et al., 2002).

For pure screw dislocations only the slip system $a\{-12-10\}\{-2021\}$ (see Fig. 1) satisfies the criteria of an a -axis misorientation axis normal to the slip plane. However, $a\{-2021\}$ is a system of relatively minor importance. Furthermore, to build twist boundaries by screw dislocations two different sets of Burgers vectors have to be simultaneously active (Hull and Bacon, 1984). This slip system does not have two Burgers vectors.

Alternatively we can model the misorientation in terms of edge dislocations. Two different edge dislocation systems could give rise to the observed dispersion around $\langle a \rangle$: $r\{10-14\}\{-2021\}$ or $f\{-1012\}\{10-11\}$. De Bresser and Spiers (1997) reported extensive activation of both of these slip systems in experimentally deformed single crystals. To resolve the ambiguities in slip systems we assess the relative activity of possible slip systems by representing their Schmid factors in the orientation map (Fig. 12). The Schmid factor indicates, for each point, the critical resolved shear stress for the slip system with respect to the local stress field (recalculated from the porphyroclast

Microstructure B

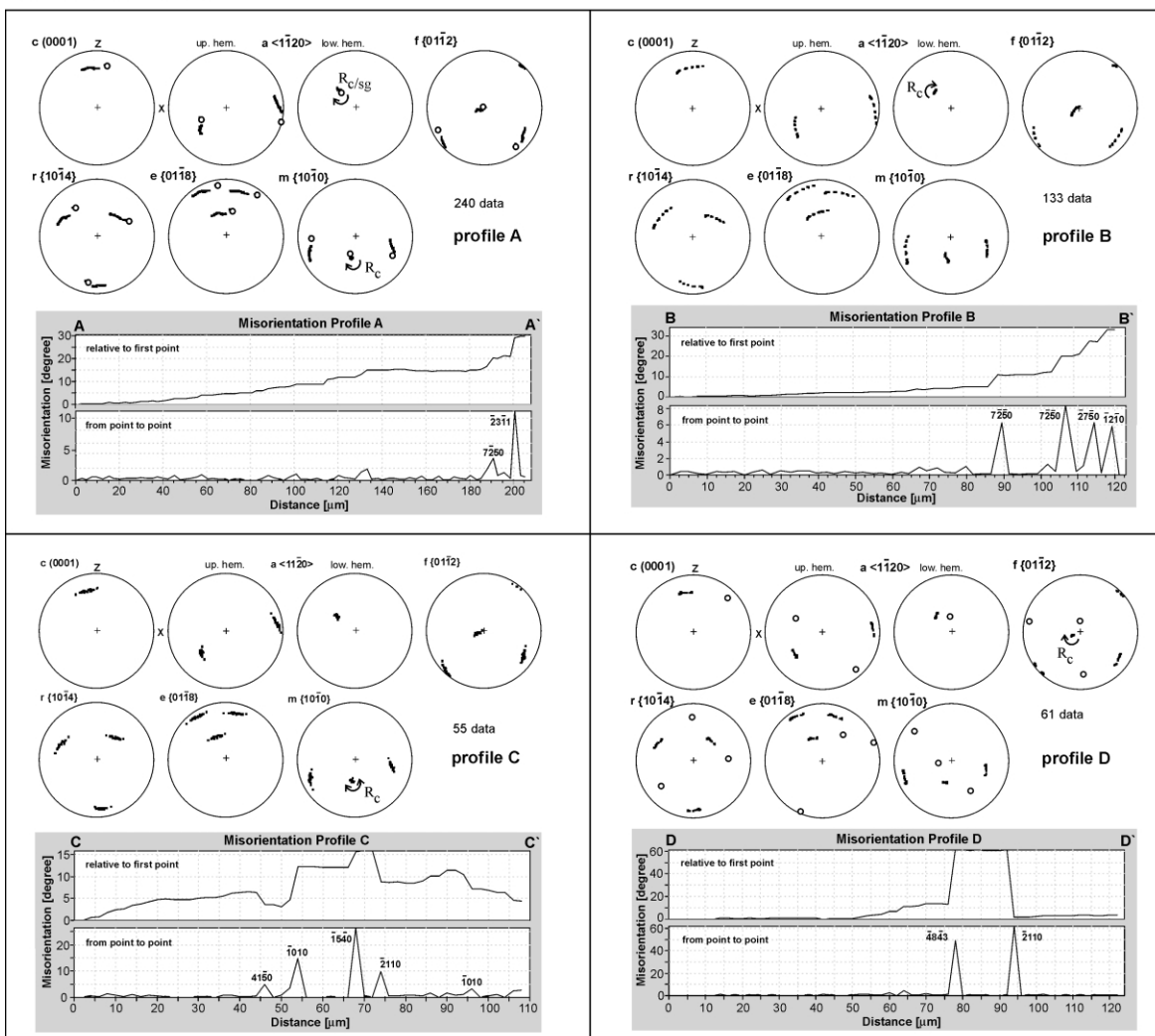


Fig. 11. Misorientation profiles within microstructure B. For description see Fig. 9. Location of profiles are given in Fig. 5.

twin geometry after Turner (1953)). The twin and host orientation domains rotate from a favourable position of easy slip outside of the microshear zone into a less favoured orientation within the high distortion area for $f\langle 10 - 11 \rangle$ slip (Fig. 12b). If slip systems approach orientations with

higher Schmid factors with progressive deformation (Schmid and Casey, 1986) $f\langle 10 - 11 \rangle$ slip seems unlikely. Since deformation in the twin domain is more intense (Fig. 3) than in the host domain, slip on $r\langle - 2021 \rangle$ explains in a better way a continuous crystal rotation of the twin

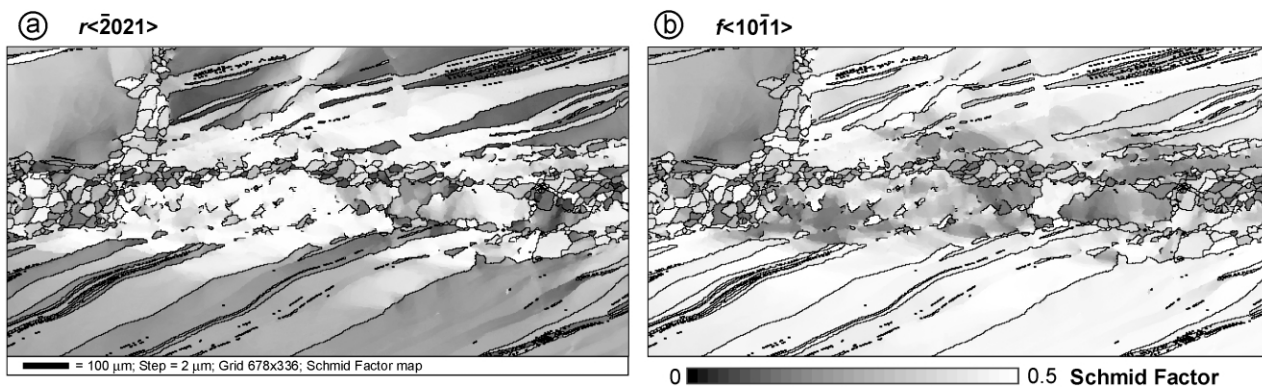


Fig. 12. Schmid factor map for microstructure A related to slip on (a) $r\langle - 2021 \rangle$ and on (b) $f\langle 10 - 11 \rangle$. Light shades indicates high Schmid factors (soft orientation), dark shades low Schmid factor (hard orientation) (see also text).

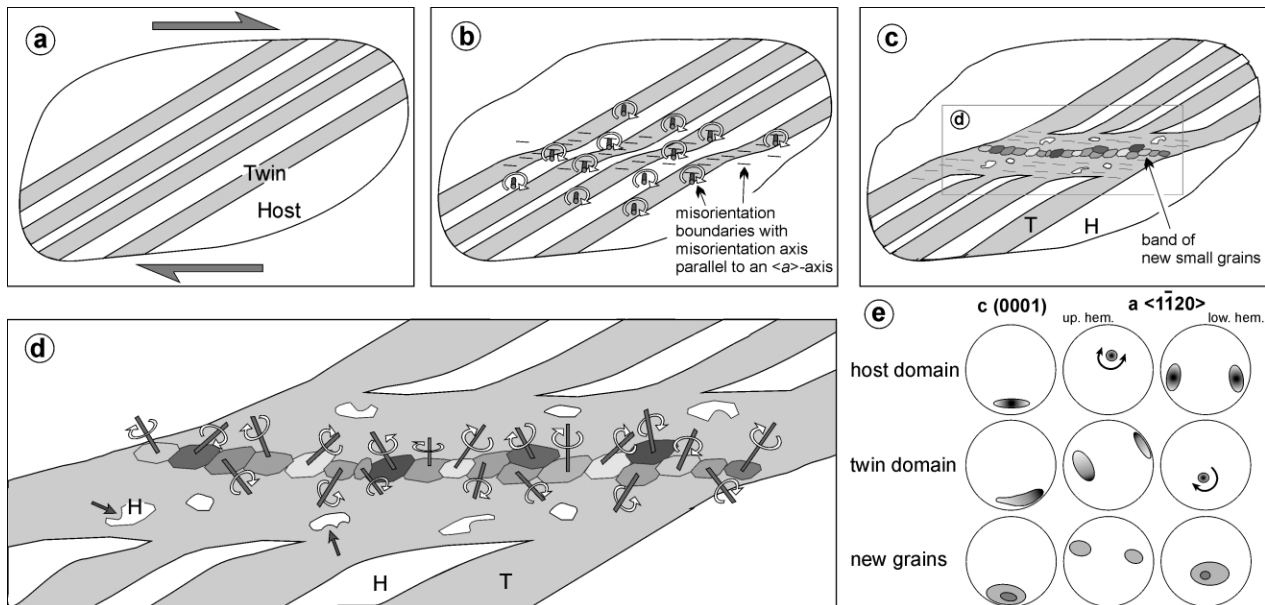


Fig. 13. Schematic model of the evolution of the intragranular microshear zone of microstructure A. (a) Calcite grain with one dominant twin system, produced by a non-coaxial deformation. (b) Intragranular strain localisation causes lattice bending and the development of low angle boundaries. (c) and (d) New small grains develop within the centre of the deformation zone by subgrain rotation. (d) Blow up of the deformation zone. Within the highly-distorted area concave grain boundaries of relicts of the host domain (H) indicate grain boundary migration (see arrow). The new grains show a random distribution of misorientation axes with respect to the surrounding host grain. (e) Pole figures give schematically the orientation dispersion of the host and twin domain (+ dispersion axes; dark shaded areas represent low-strained part) of the deformed porphyroclast and the CPO of the new grains.

domain towards an orientation of easier slip with progressive deformation (Fig. 12a).

Another way to produce a specific misorientation axis is by coupled activity in two coplanar directions. If, for example, duplex slip occurred on the basal plane $c(0001)$ in different but energetically equivalent $-a$ and $+a$ -directions (as inferred for the ultramylonite from the same marble shear zone; Bestmann et al., 2000), so that the resultant slip vector is normal to an m -plane, then a rotation around $\langle a \rangle$ could result. Production of a precisely defined misorientation axis requires equal contribution of both slip directions, which seems unlikely.

4.1.2. Microstructure B

There are three misorientation axes identified in the porphyroclast. Rotation normal to an m -plane can be best explained by one type of basal- a edge dislocation. Dispersion patterns with a misorientation axis normal to an f -plane cannot be constrained by simple dislocation models and a more complex model, involving a combination of screw and edge dislocation may be needed to explain these data. Slip systems that may generate misorientation axes around $\langle a \rangle$ are already discussed for microstructure A.

The difference in dispersion for different misorientation profiles and the occurrence of different misorientation boundaries within one orientation domain suggest that a combination of different types of dislocation were active (see also Leiss and Barber, 1999).

4.2. Deformation, recovery and recrystallization mechanisms

Deformation involving strain localization is often characterized by zones with smaller grain sizes than the surrounding area (e.g. Schmid et al., 1980; White et al., 1980; Tullis and Yund, 1985). The occurrence of intragranular small grains in calcite marble has been reported from experimentally and naturally deformed samples. The small grains develop preferentially along deformation bands and kink bands (Schmid et al., 1980; Vernon, 1981). Grain boundary migration and subgrain rotation are the two basic processes that are involved in the development of new small grains during crystal-plastic deformation of rocks (Hobbs, 1968; Urai et al., 1986; Drury and Urai, 1990).

4.2.1. Recovery, subgrain rotation and subgrain rotation recrystallization

In microstructure A, orientation dispersion, low angle boundaries and some high angle boundaries (those in the porphyroclast) share the same misorientation axis (Fig. 13b). Therefore it seems reasonable that, with increasing strain, recovery has formed subgrain walls (low angle boundaries) and that further strain has produced a continuous increase in misorientations by subgrain rotation (Fig. 14b). The sizes of the cells surrounded by low angle boundaries, in the most deformed part of the porphyroclast, are similar to the sizes of the new small grains, consistent with subgrain rotation recrystallization (Fig. 14c).

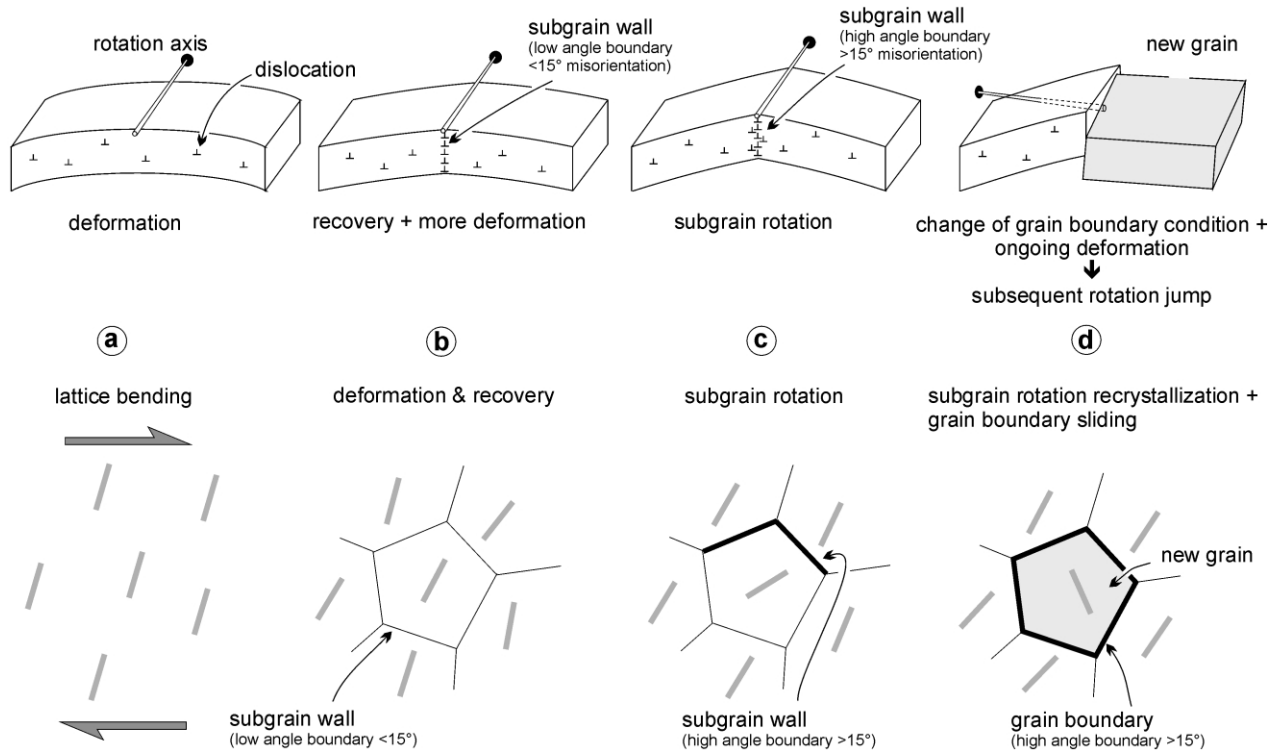


Fig. 14. Schematic model to show the development of new grains within the porphyroclast with increasing strain. (a) Gradual lattice bending around a specific rotation axis. (b) Recovery of dislocations into subgrain walls during ongoing deformation. (c) Subgrain rotation. (d) With increasing input of dislocations into the existing subgrain walls, the nature of the boundary changes. Ongoing strain may involve diffusion accommodated grain boundary sliding of the newly developed grains. As a result, the new grain loses its geometrical relationship to the host grain. Thick grey lines in the lower row show lattice orientations (schematically).

The evidence for subgrain rotation recrystallization is less clear in microstructure B. Although the slip systems appear more complex it seems reasonable that recovery has produced the low angle boundaries observed in the porphyroclast and that subgrain rotation has increased the misorientation on some of these. Subgrains are approximately the same size as new grains, again consistent with subgrain rotation recrystallization. Compared with microstructure A, many of the new grains are surrounded by relatively strain free domains of the host crystal. Thus, if our explanation is correct, deformation, recovery, subgrain rotation and subgrain rotation recrystallization have all been confined into a very narrow band.

Recovery and subgrain rotation cannot be the only deformation mechanisms in operation in these samples. These mechanisms alone cannot explain why the twin orientation domain dominates the highly-distorted area around the shear band in microstructure A. In addition recovery and subgrain rotation alone cannot explain why most misorientation angles between small new grains and their host are considerably larger than 15° and why corresponding misorientation axes are almost randomly oriented.

4.2.2. Grain (twin) boundary migration

In microstructure A, relicts of host orientation domains

with bulged grain boundaries suggest that the twin domain has consumed the host domain by grain boundary migration (Fig. 13d). Subgrain rotation associated with significant grain boundary migration is commonly observed (Drury et al., 1985; Drury and Urai, 1990; Lloyd and Freeman, 1994; Lloyd et al., 1997; Fliervoet et al., 1999).

Misorientation analysis revealed that most of the strain was accommodated in the twin domain and only to a minor part in the host domain. The Schmid factor map for $r\langle -2021 \rangle$ slip (Fig. 12a) suggests that in this case easy slip orientations (the twin domain here) developed lower dislocation densities than hard slip domains (the host domain here), which provided the driving force for twin boundary migration and the consumption of the host domain.

The small grains in both microstructures are approximately the same size as the subgrains in the deformed host. If the new grains have developed by subgrain rotation recrystallization they have not undergone significant growth by grain boundary migration.

4.2.3. Grain boundary sliding

In both microstructures, the rational misorientation axes within the deformed porphyroclast give way to sub-random misorientation axes when boundaries with new, small grains are crossed. Misorientation angles between new, small

grains and their host are large as are misorientation angles between the new grains. Large rotation angles and randomly oriented misorientation axes between porphyroclasts and recrystallized grains have been reported for various rocks, metals and ceramics (e.g. Ave Lallemand, 1985; Law, 1986; Escher and Gottstein, 1998; Kruse et al., 2001). Such an arrangement in plagioclase rocks has been referred to as no-host control (e.g. Kruse et al., 2001). No-host control seems to be inconsistent with subgrain rotation recrystallization and has been used to suggest the dominance of grain boundary migration recrystallization from nuclei (Ave Lallemand, 1985). Although there is evidence of grain boundary migration in the marble samples (Section 4.2.2), this cannot be the only process of recrystallization because the new grains are located in the interiors of old grains. Jiang et al. (2000) concluded from misorientation analysis of a low-grade albite mylonite that grain boundary sliding could be responsible for the weakening of the initially strong CPO, an increase in the mean misorientation angle between neighbouring grains and random misorientation axes.

In our study, the orientation data (see Section 4.2.1) suggest that subgrain rotation took place during strain localization and subgrain rotation recrystallization remains the best explanation for the development of new grains. In both of our microstructures the CPO of the recrystallized grains indicates an orientation relationship between the average new grain orientation and the host grain, even though individual misorientation axes are almost random (see also Hobbs, 1968). One way to explain these data is that the new grains were initially developed by subgrain rotation recrystallization, but as soon as new high angle grain boundaries were formed, they were able to undergo grain boundary sliding (Figs. 13d and 14d) (see also Fliervoet and White, 1995). The sliding process increases the average misorientation between new grains and host and between neighbouring new grains, randomises misorientation axes and weakens the CPO of the new grains. Sliding along newly developed grain boundaries might also explain why some of the new grains were rotated out of the pre-existing orientation of easy slip (Fig. 12a) (see also Herwegh et al., 1997).

4.3. Rheological implications

The possible occurrence of diffusion creep during crystal plastic deformation is extremely important. The rheologies associated with dislocation creep and diffusion creep are different. The recrystallized grains in the intracrystalline microshear zones have the same microstructure and grain size distribution as the steady state ultramylonite of the Thassos marble shear zone (Bestmann et al., 2000). The mechanistic interpretation and the rheological implications are likely to be applicable to this larger scale shear zone.

If we use the inferred deformation conditions ($T = 300\text{--}350\text{ }^{\circ}\text{C}$; Bestmann et al., 2000) and the recrystallized grain

size with the palaeopiezometer (giving $\sim 45\text{ MPa}$; Bestmann, 2000) and deformation mechanism maps ($\dot{\gamma} = 10^{-5}\text{ s}^{-1}$ and $3 \times 10^{-14}\text{ s}^{-1}$) shown by Rutter (1995), then the recrystallized grains in this sample fall into the grain-size-sensitive field whilst the porphyroclasts fall in the dislocation creep/twinning fields. It seems reasonable then that grain size reduction by dynamic recrystallization and associated strain localization leads to a decrease in the importance of grain-size-insensitive (GSI) dislocation creep relative to grain-size-sensitive (GSS) diffusion-accommodated grain boundary sliding. Whether this change caused a discrete rheological weakening (e.g. Rutter, 1995) is less clear. Deformation mechanism maps are generally constructed from mechanical data, using the assumption that the rheology is controlled entirely by the weakest mechanism. The named mechanism is not the only mechanism operating in any given field and the rheology of a material with more than one operating mechanism is not known. Specifically, we do not know whether the sharp boundaries on deformation mechanism maps should really be represented by bands of intermediate rheologies. This becomes more complex when the mechanisms are not independent: in a steady state ultramylonite, progressive grain size reduction might be balanced by grain growth at the boundary between GSI and GSS deformation mechanisms (Herwegh et al., 1997; Herwegh and Handy, 1998; de Bresser et al., 2001). Perhaps the microstructural criteria that we have developed in this paper can be applied to experiments to understand better the relative contributions of GSI and GSS deformation mechanism across the boundaries in deformation mechanism maps.

5. Summary and conclusions

The microstructural analysis of intragranular shear zones in calcite porphyroclasts from a protomylonitic marble suggests that:

1. The intragranular shear zones are developed by localization of crystal plastic deformation, with associated recovery and subgrain rotation.
2. One porphyroclast deformed by slip on $r\langle -2021 \rangle$, whereas a second one deformed by slip on a combination of slip systems.
3. Bands of recrystallized grains in intragranular shear zones are developed by subgrain rotation recrystallization.
4. In one microstructure, grain boundary migration also operated in the deformation zone and led to the growth of the twin domain at the expense of the host domain in the highly-distorted area around the new recrystallized grains.
5. New, recrystallized grains have the same size as nearby subgrains indicating they have not undergone significant grain boundary migration.

6. Recrystallized grains, once formed, underwent grain boundary sliding, as evidenced by a randomisation of neighbour grain misorientation axes and a weakening of the CPO.
7. Misorientation analysis provides a method of studying a microstructure that can identify a component of grain boundary sliding, that may in turn indicate diffusion creep. Further systematic work has to be done to use misorientations to quantify the contribution of these processes.

Acknowledgements

We thank John Wheeler, Zhenting Jiang, Norio Shigematsu and Hans de Bresser for stimulating discussion. The manuscript was much improved by the reviews of Jan Tullis and Marco Herwegh and the editorial guidance of Joao Hippert. This work was funded by a DFG grant no BE 2413/1-1. The CamScan X500 was funded by HEFCE through the grant JR98LIPR. SEM consumables were funded by NERC grants GR3/11475 and NER/A/S/2001/01181. Kees Veltkamp is thanked for coating the samples.

References

- Adams, B.L., Wright, S.I., Kunze, K., 1993. Orientation imaging: the emergence of a new microscopy. *Metallurgical Transactions* 24A, 819–831.
- Adams, B.L., Dingley, D.J., Kunze, K., Wright, S.I., 1994. Orientation imaging microscopy: new possibilities for microstructural investigations using automated BKD analysis. In: Bunge, H.J. (Ed.), *Textures of Materials*. Proc. ICOTOM 10, Materials Science Forum, pp. 31–42.
- Ave Lallemant, H.G., 1985. Subgrain rotation and dynamic recrystallization of olivine, upper mantle diapirism, and extension of the Basin-and-Range Province. *Tectonophysics* 119, 89–117.
- Bestmann, M., 2000. Evolution of a shear zone in calcite marble on Thassos Island, Northern Greece: results from microfabrics and stable isotopes. *Erlanger geologische Abhandlungen* 131, 1–127.
- Bestmann, M., Kunze, K., Matthews, A., 2000. Evolution of a calcite marble shear zone complex on Thassos Island, Greece: microstructural and textural fabrics and their kinematic significance. *Journal of Structural Geology* 22, 1789–1807.
- Bunge, H.J., 1965. Zur Darstellung allgemeiner Texturen. *Zeitschrift zur Metallkunde* 56, 872.
- De Bresser, J.H.P., 1991. Intracrystalline deformation of calcite. *Geologica Ultrajectina* 79, 1–191.
- De Bresser, J.H.P., Spiers, C.J., 1997. Strength characteristics of the r, f and c slip systems in calcite. *Tectonophysics* 272, 1–23.
- De Bresser, J.H.P., ter Heere, J.H., Spiers, C.J., 2001. Grain size reduction by dynamic recrystallization: can it result in major rheological weakening. *International Journal of Earth Sciences (Geologische Rundschau)* 90, 28–45.
- Drury, M.R., Urai, J.L., 1990. Deformation-related recrystallization processes. *Tectonophysics* 172, 235–253.
- Drury, M.R., Humphreys, F.J., White, S.H., 1985. Large strain deformation studies using polycrystalline magnesium as a rock analogue, Part II. Dynamic recrystallization mechanisms at high temperatures. *Physical Earth Planetary Science* 40, 208–222.
- Escher, C., Gottstein, G., 1998. Nucleation of recrystallization in boron doped Ni₃Al. *Acta Materialia* 46, 525–539.
- Fliervoet, T.F., White, S.H., 1995. Quartz deformation in a very fine grained quartzo-feldspathic mylonite: lack of evidence for dominant grain boundary sliding deformation. *Journal of Structural Geology* 17(8), 1095–1109.
- Fliervoet, T.F., Drury, M.R., Chopra, P.N., 1999. Crystallographic preferred orientation and misorientations in some olivine rocks deformed by diffusion or dislocation creep. *Tectonophysics* 303, 1–27.
- Fynn, G.W., Powell, W.J.A., 1979. *The Cutting and Polishing of Electro-optic Materials*, Adams Hilger, London.
- Herwegh, M., Handy, M.R., 1998. The origin of shape preferred orientations in mylonite: inference from in-situ experiments of polycrystalline norcamphor. *Journal of Structural Geology* 20, 681–694.
- Herwegh, M., Handy, M.R., Heibronner, R., 1997. Temperature- and strain-rate-dependent microfabric evolution in monomineralic mylonite: evidence from in situ deformation of norcamphor. *Tectonophysics* 280, 83–106.
- Hobbs, B.E., 1968. Recrystallization of single crystal quartz. *Tectonophysics* 6, 353–401.
- Hull, D., Bacon, D.J., 1984. *Introduction to Dislocations*, Pergamon, Oxford.
- Humphreys, F.J., Bate, P.S., Hurley, P.J., 2001. Orientation averaging of EBSD data. *Journal of Microscopy* 201, 50–58.
- Jiang, Z., Prior, D., Wheeler, J., 2000. Albite crystallographic preferred orientation and grain misorientation distribution in a low-grade mylonite: implication for granular flow. *Journal of Structural Geology* 22, 1663–1674.
- Kruse, R., Stuenitz, H., Kunze, K., 2001. Dynamic recrystallization processes in plagioclase porphyroclasts. *Journal of Structural Geology* 23, 1781–1802.
- Kunze, K., Heidebach, F., Wenk, H.-R., Adams, B.L., 1994. Orientation imaging microscopy of calcite rocks. In: Bunge, H.J., Siegesmund, S., Skrotzki, W., Weber, K. (Eds.), *Textures of Geological Materials*, DGM Informationsgesellschaft, Oberusel, pp. 279–302.
- Law, R.D., 1986. Relationships between strain and quartz crystallographic fabrics in the Roche Maurice quartzites of Plougastel, western Brittany. *Journal of Structural Geology* 8, 493–515.
- Leiss, B., Barber, D.J., 1999. Mechanisms of dynamic recrystallization in naturally deformed dolomite inferred from EBSD-analyses. *Tectonophysics* 303, 51–69.
- Lloyd, G.E., Freeman, B., 1991. SEM electron channelling analysis of dynamic recrystallization in a quartz grain. *Journal of Structural Geology* 13, 945–953.
- Lloyd, G.E., Freeman, B., 1994. Dynamic recrystallization of quartz and quartzites. *Journal of Structural Geology* 16, 867–881.
- Lloyd, G.E., Farmer, A.B., Mainprice, D., 1997. Misorientation analysis and the formation and orientation of subgrain and grain boundaries. *Tectonophysics* 279, 55–78.
- Mainprice, D., Lloyd, G.E., Casey, M., 1993. Individual orientation measurements in quartz polycrystals—advantages and limitation for texture and petrophysical property determinations. *Journal of Structural Geology* 15, 1169–1187.
- Pieri, M., Kunze, K., Burlini, L., Stretton, I., Olgaard, D.L., Burg, J.-P., Wenk, H.-R., 2001. Texture development in calcite by deformation and dynamic recrystallization at 1000 K during torsion experiments of marble to large strains. *Tectonophysics* 330, 119–140.
- Prior, D.J., 1999. Problems in determining the misorientation axes, for small angular misorientations, using electron backscatter diffraction in the SEM. *Journal of Microscopy* 195, 217–225.
- Prior, D.J., Trimby, P.W., Weber, U.D., Dingley, D.J., 1996. Orientation contrast imaging of microstructures in rocks using foreshoot detectors in the scanning electron microscope. *Mineralogical Magazine* 60, 859–869.
- Prior, D.J., Boyle, A.P., Brenker, F., Cheadle, M.C., Day, A., Lopez, G., Peruzzo, L., Potts, G.J., Reddy, S.M., Spiess, R., Trimby, P.W.,

- Wheeler, J., Zetterström, L., 1999. The application of electron backscatter diffraction and orientation contrast imaging in the SEM to textural problems in rocks. *American Mineralogist* 84, 1741–1759.
- Prior, D.J., Wheeler, J., Peruzzo, L., Spiess, R., Storey, C., 2002. Some garnet microstructures: an illustration of the potential of orientation maps and misorientation analysis in microstructural studies. *Journal of Structural Geology* 24, 999–1011.
- Randle, V., Ralph, B., 1986. A practical approach to the determination of the crystallographic grain boundaries. *Journal of Material Sciences* 21, 3823–3828.
- Rutter, E.H., 1995. Experimental study of the influence of stress, temperature, and strain on the dynamic recrystallization of Carrara marble. *Journal of Geophysical Research* 100, 24651–24663.
- Schmid, S.M., Casey, M., 1986. Complete fabric analysis of some commonly observed quartz C-axis patterns. *Geophysical Monographs* 36, 263–286.
- Schmid, S.M., Paterson, M.S., Boland, J.N., 1980. High temperature flow and dynamic recrystallization in Carrara marble. *Tectonophysics* 65, 245–280.
- Spiess, R., Peruzzo, L., Prior, D.J., Wheeler, J., 2001. Development of garnet porphyroblasts by multiple nucleation, coalescence and boundary misorientation driven rotations. *Journal of Metamorphic Geology* 19, 269–290.
- Trepied, L., Doukhan, J.C., Paquet, J., 1980. Subgrain boundaries in quartz. Theoretical analysis and microscopic observations. *Physics and Chemistry of Minerals* 5, 201–218.
- Trimby, P.W., Prior, D.J., Wheeler, J., 1998. Grain boundary hierarchy development in a quartz mylonite. *Journal of Structural Geology* 20, 917–935.
- Trimby, P.W., Drury, M.R., Spiers, J., 2000. Recognising the crystallographic signature of recrystallization processes in deformed rocks: a study of experimentally deformed rocksalt. *Journal of Structural Geology* 22, 1609–1620.
- Tullis, J., Yund, R.A., 1985. Dynamic recrystallization of feldspar: a mechanism for ductile shear zone formation. *Geology* 13, 238–241.
- Turner, F.J., 1953. Nature and dynamic interpretation of deformation in calcite of three marbles. *American Journal of Science* 251, 276–298.
- Urai, J.L., Means, W.D., Lister, G.S., 1986. Dynamic recrystallization of minerals. In: Hobbs, B.E., Heard, H.C. (Eds.), *Mineral and Rock Deformation: Laboratory Studies (the Paterson Volume)*. *Geophysical Monograph of American Geophysical Union* 36, pp. 161–200.
- Vernon, R.H., 1981. Optical microstructures of partly recrystallized calcite in some naturally deformed marbles. *Tectonophysics* 78, 601–612.
- Wheeler, J., Prior, D.J., Jiang, Z., Spiess, R., Trimby, P.J., 2001. The petrological significance of misorientations between grains. *Contribution to Mineralogy and Petrology* 141, 109–124.
- White, S.H., Burrows, S.E., Carreras, J., Shaw, N.D., Humphreys, F.J., 1980. On mylonites in ductile shear zones. *Journal of Structural Geology* 2, 175–185.